A New Universal Approach to Time Domain Modeling and Simulation of UWB Channel Containing Convex Obstacles Using Vector Fitting Algorithm

P. Górniak, *Poznan University of Technology*, W. Bandurski, *Poznan University of Technology*

***Abstract*—The paper presents a new approach to time domain modeling of UWB channels with multiple convex obstacles. Rational approximation exploiting the vector fitting algorithm (VF) is used for deriving the closed form impulse response of a multiple diffraction ray creeping on a cascade of convex obstacles. The VF algorithm is performed with respect to new generalized variables proportional to frequency but also taking into account geometrical parameters of the obstacles. The limits of the approximation domain for the VF algorithm reflect the range of ultra-wideband (UWB) channel parameters that can be met in practical UWB channel scenarios. The results of VF approximation have the form of a finite series of partial fractions in the frequency domain, which next is easily transformed to the time domain. Obtained in this way impulse response is a sum of exponential functions. As a consequence, in simulations of electromagnetic (EM) wave propagation we can implement very fast and effective convolution algorithms with any input signal or perform simulations implementing SPICE-like programs.**

***Index Terms*— ultra-wideband, vector fitting, time domain, conducting cylinder, uniform theory of diffraction**

I. Introduction

Ultra-wideband (UWB) technology enables many beneficial possibilities in data transmission and radar area [1]. In order to take advantage of these possibilities, careful analysis of a given UWB system is required, in particular analysis of the propagation channel. The natural choice of the domain for the UWB propagation channel analysis is the time domain with the usage of the impulse responses concept. The impulse response of the propagation channel can be determined from the measurements, numerical computations or in an analytical way.

We focus our considerations on effective time domain modeling of UWB channels that comprise obstacles (e.g. people) which can be modeled by convex objects (cylinders in the 3D case or ovals in the 2D case). The EM wave hitting an obstacle can be reflected, diffracted or it can pass through this obstacle. Our aim is to present the method for obtaining a simple, closed form impulse response which can mathematically describe such phenomena. For the sake of clarity and simplicity of the description of this approach we consider the diffraction case only. We use the Uniform Theory of Diffraction (UTD) in our analysis. In the paper we give a simple, closed form impulse response for the multiple diffraction creeping ray, as well as the procedure for obtaining it.

The analytical description of the propagation of the EM wave on convex objects in the time and the frequency domain was already considered in the literature for the case of a single obstacle [2] – [5], as well as a cascade of convex obstacles, e.g. [6]. The disadvantage of these solutions is their high complexity which can result in very long time of computation.

This issue has been also considered by the present authors in [7, 8], where two solutions of this problem were proposed. The first solution was an analytical solution which consisted in channel transfer function transformation from the frequency domain to the time domain. As a result we obtained two formulas valid for different ranges of parameter $\xi_d(\omega, a, b, \theta)$ [7, 8]. The first formula was valid in the range $0<\xi_d<\xi_{dth}$, and the second in the range $\xi_{dth}<\xi_d<\infty$. The first one referred to the case of diffraction ray traveling (creeping) along shorter distances while the second one referred to the diffraction ray traveling along greater distances, as in radar applications [9] – [12]. We had to check whether the values of ξ_d for a given diffraction ray scenario fulfilled the requirements for the application of the first or the second formula. For this reason, and because of complex calculation procedures, this approach can be too difficult to implement for more complex channel scenarios.

The second solution consisted in rational approximation of the channel transfer function in the frequency domain by means of the vector fitting (VF) algorithm [13]. As a result we obtained an impulse response in the form of a sum of exponential functions [7]. This solution allowed us to model a channel in SPICE-like simulators. The disadvantage of this approach was the need to approximate the channel transfer function (using the VF algorithm) for each change of the geometry of the channel and frequency band.

The paper was submitted for review on 21-OCT-2013. This work was supported by public funds in the years 2012-2014.

P. Górniak is with the Poznań University of Technology, Faculty of Electronics and Telecommunications (e-mail: pgorniak@et.put.poznan.pl).

W. Bandurski is with the Poznań University of Technology, Faculty of Electronics and Telecommunications (e-mail: wojciech.bandurski @put.poznan.pl).

In this paper, we introduce a universal rational approximation, valid for cases of diffraction rays creeping along short as well as long distances, while the obtained coefficients (poles and residues) are independent of geometry of the objects in the cascade, and of the frequency band. For this purpose, we introduce new variables for which we carry out universal rational function approximation by means of the VF algorithm. These new variables depend on the frequency and the geometry of objects in the cascade (constituting the UWB channel). Using this approach we have to perform the rational approximation once. The obtained coefficients can be then used in many other scenarios and frequency ranges. In this way we obtain a universal approximation of the transfer function of the channel containing convex objects that can be used for all considered scenarios of the channel and frequency band (of course in reasonable limits). For more details see Section 3.

The rest of the paper is organized as follows. In Section 2 we revise the concept of the UTD transfer function for a creeping ray. In section 3 we describe the procedure of obtaining the closed form universal rational approximation of the transfer function of a creeping ray. Simulation of the channel consisting of a cascade of convex objects in a SPICE simulator is shown in Section 4. In section 5 some examples are given. Section 6 concludes the paper.

II. THE UTD CREEPING RAY UNIVERSAL TRANSFER FUNCTION

The case of one multiple diffraction ray that creeps on a cascade of convex obstacles in the form of elliptical or circular 2D conducting cylinders is shown in Fig. 1. The solid line relates to the amplitude diffraction while the dotted line indicates slope diffraction [6, 7]. We assume that slope diffraction originates after the first obstacle and is not taken into consideration after the last obstacle. We assume that the observation point (receiving antenna) is in the far zone. We have first, second and N^{th} convex obstacle shown in Fig. 1.

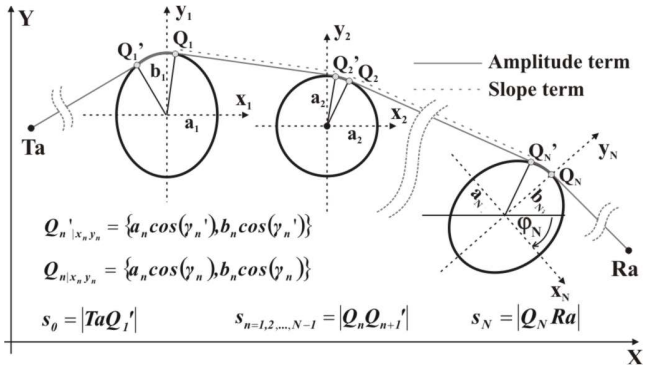

Fig. 1. A multiple diffraction ray creeping on N convex objects; γ_n' and γ_n are the angular coordinates of points Q_n' and Q_n, respectively, measured from x_n axis.

The transmitting and receiving antennas are placed at points Ta and Ra, respectively. The attachment and shedding points are marked with Q_n' and Q_n, respectively (n=1,2,…,N). The main parameters of the scenario are: a_n and b_n – the axes of the n^{th} elliptical cylinder, γ_n' and γ_n – the parametrical coordinates of the points Q_n'and Q_n respectively.

The distances along which the EM wave propagates in the air are denoted by s_k, where s_k is the length of the ray path between object k and object k+1 (k={0,1,2,…N}). Objects denoted by 0 (for the case of k=0) and N+1 (for the case of k=N) refer to the transmitting antenna and receiving antenna respectively.

It can be shown [6] that when slope diffraction on the last convex object is not taken into account (the receiving antenna is sufficiently far from the last convex object), Fourier transforms of the electric field at the output of the transmitting antenna – $E^{Ta}(\omega)$ and at the input of the receiving antenna – $E^{Ra}(\omega)$ for one creeping ray (Fig.1) are related by the expression:

$$E^{Ra}(\omega) = E^{Ta}(\omega)\cdot H^{(N)}(\omega)\cdot exp\left(-j\cdot\frac{\omega}{v_0}\cdot s^p\right) \times A^c(s^0, s^1, \ldots, s^{N+1}), \quad (1)$$

where s_p is the total length of the creeping ray and v_o is the speed of EM wave in free space, $A_c(s_0,s_1,\ldots,s_N)$ is the product of all the spreading factors [14, 15] and $H^{(N)}(\omega)$ is the transfer function of a ray that creeps on a cascade of N (N>1) convex objects. Transfer function $H^{(N)}(\omega)$ does not include any delay factors, which however are collected in the expression $\exp(-j\omega s^p/v_o)$. For simplicity of the presentation of $H^{(N)}(\omega)$ we use the upper index N, which is the number of convex obstacles in the cascade, and only one variable, ω; other variables and parameters are hidden for the moment. The transfer function $H^{(N)}(\omega)$ can be written in the recursive form [6, 7]:

$$H^{(N)}(\omega) = H^{(N-1)}(\omega)\cdot H_{A(N)} + H_M{}^{(N-1)}(\omega)\cdot\frac{s_N\cdot v_0}{j\omega}\cdot H_{Z(N)}(\omega), \quad (2)$$

where:

$$H_M{}^{(N-1)}(\omega) = H^{(N-2)}(\omega)\cdot H_{Z(N-1)}(\omega) + H_M{}^{(N-2)}(\omega)\cdot H_{D(N-1)}(\omega), \quad (3)$$

$$H_{Z(N)}(\omega) = H_{Z(N)}(\omega,\gamma_N',\gamma_N,a_N,b_N,s_N) = \frac{1}{s_N}\cdot\frac{d}{d\varphi_N}\{H_{A(N)}(\omega,\gamma_N',\gamma_N,a_N,b_N)\}, \quad (4)$$

$$H_{D(N)}(\omega) = H_{D(N)}(\omega,\gamma_N',\gamma_N,a_N,b_N,s_N) = \frac{v_0}{j\omega}\frac{d}{d\varphi_N}\{H_{Z(N)}(\omega,\gamma_N',\gamma_N,a_N,b_N,s_N)\}. \quad (5)$$

Transfer function $H_{A(n)}(\omega)$ represents the amplitude diffraction term and will be given in (11), while $H_{Z(n)}(\omega)$ and $H_{D(n)}(\omega)$ are related to the slope diffraction of the EM field [6, 16]. In order to initialize the above recursive procedure the following starting functions must be used: $H^{(0)}(\omega)=1$, $H_M{}^{(0)}(\omega)=0$.

Let us consider the case N = 3. Then we have:

$$H^{(3)}(\omega) = H_{A(1)}(\omega)H_{A(2)}(\omega)H_{A(3)}(\omega) + \frac{s_2 v_o}{j\omega}H_{Z(1)}(\omega)H_{Z(2)}(\omega)H_{A(3)}(\omega) + \quad (6)$$

$$\frac{s_3 \mathrm{v_o}}{j\omega}\Big(H_{A(1)}(\omega)H_{Z(2)}H_{Z(3)}(\omega) + H_{Z(1)}(\omega)H_{D(2)}(\omega)H_{Z(3)}(\omega)\Big).$$

In formulas (3) – (5) we use the lower index n in functions $H_{A(n)}(\omega)$, $H_{Z(n)}(\omega)$ and $H_{D(n)}(\omega)$. The lower index n is dedicated to functions or arguments determined for the n^{th} convex object in a cascade, see Fig. 1. Functions $H_{A(n)}(\omega)$, $H_{Z(n)}(\omega)$ and $H_{D(n)}(\omega)$ include variables: s_n, γ_n' and γ_n and parameters: a_n, b_n, $L_{d(n)}$ and $L_{Z(n)}$, which are hidden at present for the sake of clarity, but will be used when necessary.

The amplitude term $H_{A(n)}(\omega)$ in the transfer function $H^{(N)}(\omega)$ (diffraction coefficient in physical sense) for a separate n^{th} convex object in a cascade, after manipulations and substitutions, can be presented in the following way [7, 15]:

$$H_{A(n)}(\omega) = H_{A1(n)}(\omega) + H_{A2(n)}(\omega)\,, \tag{7}$$

where:

$$H_{A1(n)}(\omega) = AmpAT_n \cdot exp\left(-j\frac{\pi}{4}\right)\frac{F_T\left(X_{d(n)}\right)}{\sqrt{X_{d(n)}}}, \tag{8}$$

$$H_{A2(n)}(\omega) = AmpAF_n \times \left[-exp\left(-j\frac{\pi}{4}\right)\frac{\begin{Bmatrix}p^*(\xi_{d(n)})\\ q^*(\xi_{d(n)})\end{Bmatrix}}{\sqrt{\xi_{d(n)}}}\right], \tag{9}$$

$$X_{d(n)} = \frac{\omega L_{d(n)}{\theta_n}^2}{2V_0}, \tag{10}$$

$$\xi_{d(n)} = \left(\frac{\omega \cdot R_n}{2\mathrm{v_0}}\right)^{1/3} \cdot \theta_n\,, \tag{11}$$

$$\theta_n = a_n b_n F_{c(n)}\sqrt{T_{c(n)}}\,, \tag{12}$$

$$R_n = \left(\frac{1}{\sqrt{T_{c(n)}}}\right)^3 \cdot \frac{1}{a_n b_n}. \tag{13}$$

$$AmpAT_n = \sqrt{\frac{L_{d(n)}}{4\pi}}, \tag{14}$$

$$AmpAF_n = \sqrt{\frac{F_{c(n)}}{T_{c(n)}}}. \tag{15}$$

The separation factor $L_{d(n)}$ is given in [6, 14, 15] while definitions of variables $T_{c(n)}$ and $F_{c(n)}$ can be found in APPENDIX I of the paper.

It should be noted that when $a_n = b_n$ (circular cylinder case), parameter R_n is the radius of the circular cylinder and θ_n is the angular distance along which a diffraction ray creeps.

$F_T(X_{d(n)})$ in (8) is the transition function [14, 15], while $p^*(\xi_d)$ and $q^*(\xi_d)$ are Fock scattering functions for the TM polarisation case and for the TE polarisation case, respectively [14, 15].

In order to find the universal VF approximation of $H_{A(n)}(\omega)$, $H_{Z(n)}(\omega)$ and $H_{D(n)}(\omega)$ dedicated to general, practical UWB scenarios, we rearrange $H_{A(N)}(\omega)$ into a function of variables $X_{d(n)}$ and a new variable $\xi_{dsub(n)}$, which is given by:

$$\xi_{dsub(n)} = \frac{\omega \cdot R_n}{2\mathrm{v_0}} \cdot {\theta_n}^3\,. \tag{16}$$

Now the components of (11) obtain the following form:

$$H_{A1(n)}\left(X_{d(n)}\right) = AmpAT_n \times exp\left(-j\frac{\pi}{4}\right)\frac{F_T\left(X_{d(n)}\right)}{\sqrt{X_{d(n)}}} = AmpAT_n \cdot V_{T1}\left(X_{d(n)}\right), \tag{17}$$

$$H_{A2(n)}\left(\xi_{dsub(n)}\right) = AmpAF_n \cdot \left[-exp\left(-j\frac{\pi}{4}\right)\frac{p^*\left(\xi_{dsub(n)}{}^{1/3}\right)}{\sqrt{\xi_{dsub(n)}{}^{1/3}}}\right] = AmpAF_n \cdot V_{F1}\left(\xi_{dsub(n)}\right). \tag{18}$$

For the sake of clarity and simplicity of further considerations we choose only one polarization of the EM wave. Therefore we assume that the electric field of the propagating wave is tangential to the cylinders. Consequently we use only $p^*(\xi_d)$ in (18) and in the rest of the paper.

After performing all necessary manipulations in (17) and (18) according to (4) we obtain two components of $H_{Z(n)}(\omega)$. The first has the form shown in (19). We can see that for the slope diffraction case $X_{d(n)}$ is changed into $X_{Z(n)}$ [6, 7] and the separation factor $L_{d(n)}$ into $L_{Z(n)}$ [6, 7], respectively:

$$H_{Z1(n)}\left(X_{Z(n)}\right) = \frac{1}{s_N}\cdot\frac{d}{d\varphi_N}\left\{H_{A1(N)}\left(X_{Z(n)}\right)\right\} = \frac{j\omega}{s_n\cdot[\varphi(\gamma_n)]'} \times \left[AmpZT_{1(n)} \cdot V_{T1}\left(X_{Z(n)}\right) + AmpZT_{2(n)} \cdot V_{T2}(\omega)\right], \tag{19}$$

where:

$$AmpZT_{1(n)} = \sqrt{\frac{{L_{Z(n)}}^3}{\pi}}\,{G_{c(n)}}^2 K_{11(n)}\,, \tag{20}$$

$$AmpZT_{2(n)} = -\frac{L_{Z(n)}}{\sqrt{\pi}}\,G_{c(n)}K_{11(n)}\,. \tag{21}$$

The second component of $H_{Z(n)}(X_{Z(n)},\xi_{d(n)})$, obtained from (4), is given by:

$$H_{Z2(N)}\left(\xi_{dsub(n)}\right) = \frac{1}{s_N}\cdot\frac{d}{d\varphi_N}\left\{H_{A2(N)}\left(\xi_{dsub(n)}\right)\right\} = \frac{AmpZF_{1(n)}}{s_n\cdot[\varphi(\gamma_n)]'}\cdot V_{F1}\left(\xi_{dsub(n)}\right) + \frac{AmpZF_{2(n)}}{s_n\cdot[\varphi(\gamma_n)]'}\cdot V_{F2}\left(\xi_{dsub(n)}\right), \tag{22}$$

where:

$$AmpZF_{1(n)} = |sin(2\gamma_n)|\left({a_n}^2 - {b_n}^2\right) \times \frac{\left\{[a_n sin(\gamma_n')]^2 + [b_n cos(\gamma_n')]^2\right\}^{1/4}\sqrt{F_{c(n)}}}{4\cdot\{[a_n sin(\gamma_n)]^2 + [b_n cos(\gamma_n)]^2\}^{3/4}}, \tag{23}$$

$$AmpZF_{2(n)} = \frac{\{[a_n sin(\gamma_n')]^2 + [b_n cos(\gamma_n')]^2\}^{1/4}}{\{[a_n sin(\gamma_n)]^2 + [b_n cos(\gamma_n)]^2\}^{1/4}\sqrt{F_{c(n)}}}. \quad (24)$$

The definitions of variables $G_{c(n)}$ and $K_{11(n)}$ can be found in APPENDIX I of the paper while $[\varphi_n(\gamma_n)]'$ denotes the first order derivative of φ_n with respect to γ_n. Applying now (5) to (26) and (33) we obtain two components of $H_{D(n)}(X_{Z(n)},\xi_{d(n)})$. The first of them takes the form:

$$H_{D1(n)}(X_{Z(n)}) = \frac{v_0}{j\omega}\frac{d}{d\varphi_n}\{H_{Z1(N)}(X_{Z(n)})\} = \frac{1}{\{[\varphi(\gamma_n)]'\}^2}\times \left[H_{d1(n)}(X_{Z(n)}) - \frac{[\varphi(\gamma_n)]''}{[\varphi(\gamma_n)]'}H_{Z1(N)}(X_{Z(n)})\right], \quad (25)$$

where:

$$H_{d1(n)}(X_{Z(n)}) = \frac{v_0}{s_n}\times \{[AmpDT_{11(n)} + j\omega\cdot AmpDT_{12(n)}]\cdot V_{T1(n)}(X_{Z(n)}) + [AmpDT_{21(n)} + j\omega\cdot AmpDT_{22(n)}]\cdot V_{T2(n)}(X_{Z(n)})\} \quad (26)$$

$$AmpDT_{11(n)} = \sqrt{\frac{L_{Z(n)}{}^3}{\pi}}G_{c(n)}{}^2(2K_{11(n)}{}^2 + K_{12(n)}), \quad (27)$$

$$AmpDT_{12(n)} = 2\sqrt{\frac{L_{Z(n)}{}^5}{\pi}}G_{c(n)}{}^4K_{11(n)}{}^2, \quad (28)$$

$$AmpDT_{21(n)} = -\frac{L_{Z(n)}}{\sqrt{\pi}}G_{c(n)}(K_{11(n)}{}^2 + K_{12(n)}), \quad (29)$$

$$AmpDT_{22(n)} = -2\frac{L_{Z(n)}{}^2}{\sqrt{\pi}}G_{c(n)}{}^3K_{11(n)}{}^2, \quad (30)$$

and $[\varphi_n(\gamma_n)]''$ denotes the second order derivative of φ_n with respect to γ_n, while the other is given by:

$$H_{D2(N)}(\xi_{dsub(n)}) = \frac{v_0}{j\omega}\frac{d}{d\varphi_n}\{H_{Z2(N)}(\xi_{dsub(n)})\} = \frac{1}{\{[\varphi(\gamma_n)]'\}^2}\times \left[H_{d2(n)}(X_{Z(n)}) - \frac{[\varphi(\gamma_n)]''}{[\varphi(\gamma_n)]'}H_{Z2(N)}(X_{Z(n)})\right], \quad (31)$$

where:

$$H_{d2(n)}(X_{Z(n)}) = \frac{v_0}{s_n j\omega}\times [AmpDF_{1(n)}V_{F1}(\xi_{dsub(n)}) + AmpDF_{3(n)}V_{F3}(\xi_{dsub(n)})] \quad (32)$$

$$AmpDF_{1(n)} = \frac{(a_n{}^2 - b_n{}^2)\sqrt{F_{c(n)}}K_{2(n)}}{4}\times \times \{[a_n sin(\gamma_n')]^2 + [b_n cos(\gamma_n')]^2\}^{1/4}, \quad (33)$$

$$AmpDF_{3(n)} = \frac{\{[a_n sin(\gamma_n')]^2 + [b_n cos(\gamma_n')]^2\}^{1/4}}{\{[a_n sin(\gamma_n)]^2 + [b_n cos(\gamma_n)]^2\}^{3/4}F_{c(n)}{}^{3/2}}. \quad (34)$$

The definitions of variables $K_{12(n)}$ in (29) and $K_{2(n)}$ in (33) can be found in APPENDIX I of the paper.

III. VF APPROXIMATION

The idea of our universal rational function approximation can be illustrated by the following simple example:

$$\widehat{H}(\omega) = A_0\sqrt{sinh(\alpha^2\omega/\beta)} \Rightarrow \widehat{H_1}(\Omega) = \frac{\widehat{H}(\Omega)}{A_0} = \sqrt{\sinh(\Omega)}, \quad \Omega = \frac{\alpha^2\omega}{\beta}.$$

After an approximation, we get:

$$\widehat{H_1}(\Omega) = \sum_k \frac{A_k}{j\Omega + B_k} \; for \; \Omega_{min} \le \Omega = \frac{\alpha^2\omega}{\beta} \le \Omega_{max},$$

or

$$\widehat{H}(\omega) \approx A_0\widehat{H_1}\left(\frac{\alpha^2\omega}{\beta}\right) = A_0\sum_k \frac{A_k\frac{\beta}{\alpha^2}}{j\omega + B_k\frac{\beta}{\alpha^2}}, \quad \Omega_{min} \le \Omega = \frac{\alpha^2\omega}{\beta} \le \Omega_{max}.$$

It means that for frequency range ($f_L \le f \le f_H$), the variable (parameter) $x=\Omega/\omega$ fulfills the following relationship

$$\frac{\Omega_{min}}{2\pi f_L} \le x = \frac{\Omega}{\omega} = \frac{\alpha^2}{\beta} \le \frac{\Omega_{max}}{2\pi f_H},$$

and for new values of parameters α, β, but fulfilling the above inequality, approximation (A_k, B_k) is still valid. In our approach, we have to approximate more than one transfer function, so we introduced more generalized variables. Equations (17) and (18), (19) and (22), (25) and (31) define the components of functions $H_{A(n)}(X_{d(n)}, \xi_{dsub(n)})$, $H_{Z(n)}(X_{Z(n)}, \xi_{dsub(n)})$, $H_{D(n)}(X_{Z(n)}, \xi_{dsub(n)})$ respectively. There are five functions of different arguments: $V_{T1}(X_{d(n)})$, $V_{T1}(X_{Z(n)})$, $V_{T2}(X_{d(n)})$, $V_{T2}(X_{Z(n)})$, $V_{F1}(\xi_{dsub(n)})$, $V_{F2}(\xi_{dsub(n)})$, $V_{F3}(\xi_{dsub(n)})$, which are to be approximated with VF. In order to apply VF approximation we must determine the ranges of variables $X_{d(n)}$, $X_{Z(n)}$ and $\xi_{d(n)}$. These ranges should reflect the values of the UWB channel parameters that can be met in a real scenario.

First we focus on convex objects which may model humans in an UWB channel. These objects can be cylinders with circular or ellipsoidal cross section with parameter R_n (13) in the range $0.2 \le R_n \le 0.3$ [m] - compare [17, 18]. The remaining parameters whose ranges must be found are frequency f, parameter θ_n (12) and the separation coefficients $L_{d(n)}$ and $L_{Z(n)}$ [6, 7]. We assume that $0.5 \le f \le 10$ [GHz] (typical UWB spectrum), $10^{-4} \le \theta_n \le \pi$ [rad] (from the practically grazing incidence case to the backscattering case) and that both values of separation coefficients, $L_{d(n)}$ and $L_{Z(n)}$, are in the range from 0.5 to 5 [m] (typical separation factor values for indoor scenarios).

With the above assumed bounds for UWB channel scenario parameters the limits of the new approximation variables are as follows: $10^{-8} \le X_{d(n)}, X_{Z(n)} \le 10^{3}$, $10^{-11} \le \xi_{dsub(n)} \le 10^{3}$. The VF algorithm yields the best results when log scale sampling of approximation domains is used.

Using (35), (36) and (37) as new variables, we can present the results of VF approximations as a series of partial fractions. The approximate forms of the components of $H_{A(n)}(X_{d(n)},\xi_{dsub(n)})$, $H_{Z(n)}(X_{Z(n)},\xi_{dsub(n)})$, $H_{D(n)}(X_{Z(n)},\xi_{dsub(n)})$ are given by (38) – (43).

$$X_{wd(n)} = \frac{X_{d(n)}}{\omega} \tag{35}$$

$$X_{wZ(n)} = \frac{X_{Z(n)}}{\omega} \tag{36}$$

$$\xi_{wd(n)} = \frac{\xi_{dsub(n)}}{\omega} \tag{37}$$

$$\widehat{H}_{A1(n)}(\omega) = AmpAT_n \cdot \sum_{k=1}^{KT1} \frac{CT1_k \cdot X_{wd(n)}^{-1}}{j\omega + AT1_k \cdot X_{wd(n)}^{-1}} \tag{38}$$

$$\widehat{H}_{A2(n)}(\omega) = AmpAF_n \cdot \sum_{k=1}^{KF1} \frac{CF1_k \cdot \xi_{wd(n)}^{-1}}{j\omega + AF1_k \cdot \xi_{wd(n)}^{-1}} \tag{39}$$

$$\widehat{H}_{Z1(n)}(\omega) = \frac{j\omega \cdot AmpZT_{1(n)}}{s_n} \cdot \sum_{k=1}^{KT1} \frac{CT1_k \cdot X_{wZ(n)}^{-1}}{j\omega + AT1_k \cdot X_{wZ(n)}^{-1}} + \frac{j\omega \cdot AmpZT_{2(n)}}{s_n} \cdot \sum_{k=1}^{KT2} \frac{CT2_k}{j\omega + AT2_k} \tag{40}$$

$$\widehat{H}_{Z2(n)}(\omega) = \frac{AmpZF_{1(n)}}{s_n} \cdot \sum_{k=1}^{KF1} \frac{CF1_k \cdot \xi_{wd(n)}^{-1}}{j\omega + AF1_k \cdot \xi_{wd(n)}^{-1}} + \frac{AmpZF_{2(n)}}{s_n} \cdot \sum_{k=1}^{KF2} \frac{CF2_k \cdot \xi_{wd(n)}^{-1}}{j\omega + AF2_k \cdot \xi_{wd(n)}^{-1}} \tag{41}$$

$$\widehat{H}_{D1(n)}(\omega) = \frac{v_0}{s_n\{[\varphi(\gamma_n)]'\}^2}\left(AmpDT_{11(n)} + j\omega AmpDT_{12(n)}\right) \times \sum_{k=1}^{KT1} \frac{CT1_k \cdot X_{wZ(n)}^{-1}}{j\omega + AT1_k \cdot X_{wZ(n)}^{-1}} + \frac{v_0}{s_n\{[\varphi(\gamma_n)]'\}^2}\left(AmpDT_{21(n)} + j\omega \cdot AmpDT_{22(n)}\right) \times \sum_{k=1}^{KT2} \frac{CT2_k}{j\omega + AT2_k} - \frac{[\varphi(\gamma_n)]''}{\{[\varphi(\gamma_n)]'\}^3} \widehat{H}_{Z1(n)}(\omega) \tag{42}$$

$$\widehat{H}_{D2(n)}(\omega) = \frac{v_0 \cdot AmpDF_{1(n)}}{j\omega \cdot s_n\{[\varphi(\gamma_n)]'\}^2} \times \sum_{k=1}^{KF1} \frac{CF1_k \cdot \xi_{wd(n)}^{-1}}{j\omega + AF1_k \cdot \xi_{wd(n)}^{-1}} + \frac{v_0 \cdot AmpDF_{3(n)}}{j\omega \cdot s_n\{[\varphi(\gamma_n)]'\}^2} \times \sum_{k=1}^{KF3} \frac{CF3_k \cdot \xi_{wd(n)}^{-1}}{j\omega + AF3_k \cdot \xi_{wd(n)}^{-1}} - \frac{[\varphi(\gamma_n)]''}{\{[\varphi(\gamma_n)]'\}^3} \widehat{H}_{Z2(n)}(\omega) \tag{43}$$

To keep the absolute value of relative error of all rational approximations under 1.75% ($|\varepsilon(\omega)| \le 1.75\%$, see (44) defined below) for variables $X_{d(n)}$, $X_{Z(n)}$ and $\xi_{dsub(n)}$ we used the following number of poles (residues) in (38) – (43): KT1=28, KT2=26, KF1=40, KF2=35, KF3= 36. In order to calculate poles and residues we used the Matlab-based package which is placed in the website [19]. We obtained for TM polarization case the values of poles and residues, which are given in Tables I – X which are placed in APPENDIX II of the paper. The tables, contain the results which allow the reader independently performs modeling and simulation of their own scenarios (with different number of objects and with different dimensions) using poles and residua calculated by us.

The error of approximations considered by us is calculated as in (44), where $\hat{f}(\omega)$ is the approximating function. The error is sign sensitive in contrast to the standard definition of a relative error of approximation, which has a positive sign.

$$\varepsilon(\omega) = \frac{f(\omega) - \hat{f}(\omega)}{f(\omega)} \cdot 100 \tag{44}$$

In order to illustrate how the error depends on and how it is sensitive to the frequency and the geometrical parameters of the telecommunication channel, we consider four sample scenarios. In our discussion, we focus on the transfer function of $H_{A(n)}(\omega)$, as the remaining transfer functions behave similarly.

In Figs. 2a) and 2b), we presented the frequency dependence of approximation error of real and imaginary part of $H_{A(n)}(\omega)$, respectively, while Figs. 2c) and 2d) show the frequency dependence of approximation variables, $X_{d(n)}$ and $\xi_{dsub(n)}$, respectively. The frequency range is 0.32-10GHz. In each of the figures, we have 4 functions of frequency related to 4 different geometries of a creeping ray scenario. Such examples aptly illustrate the dependence of the approximation error on geometrical parameters of the creeping ray scenario and show the importance of keeping the values of approximation variables within the range of approximation.

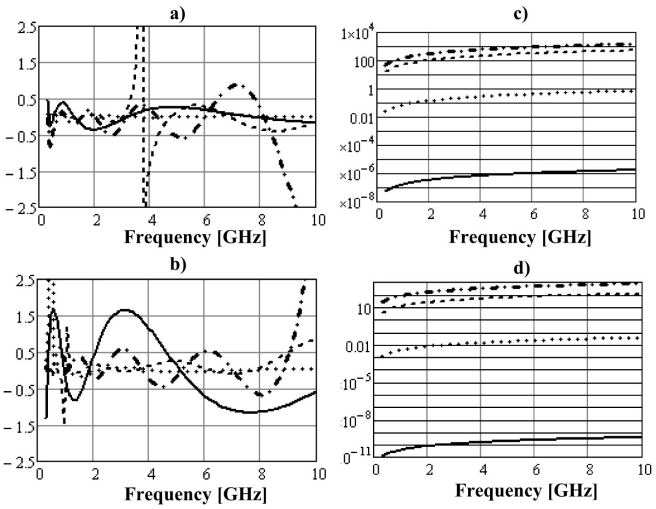

Fig. 2. The functions of the approximation error of the real (a) and imaginary (b) part of $H_{A(n)}(\omega)$ and the characteristics of $X_{d(n)}$ (c) and $\xi_{dsub(n)}$ (d) with respect to frequency in the range of 0.32-10 GHz for scenarios: 1st – solid line, 2nd – dotted line, 3rd – dash line, 4th – dash-dott line.

The approximation variables are most sensitive to the variations of the angle distance along which a diffraction ray travels, parameter θ_n. Therefore, in the geometry scenarios, we change this distance while keeping the values of other parameters in a narrow range. The results related to the 1st, 2nd, 3rd and 4th scenario are shown with solid line, dotted line, dash line and dash-dott line, respectively. In the 1st scenario, we have a case of practically grazing incidence. The values of a_n, b_n, γ_n, γ_n' and $L_{d(n)}$ equal 0.35m, 0.5m, 0.51rad, 0.51023rad and 0.5m, respectively. The same parameters in the 2nd scenario assume the respective values of 0.25m, 0.3m, 1.4rad, 1.5rad and 0.5m. For the 3rd scenario, these values are changed to 0.25m, 0.3m, 1.5rad, 3.1rad and 1.5m, respectively, while in scenario no. 4, to 0.25m, 0.2m, 0.1rad, 3.542rad and 1.25m, respectively. In the 4th scenario, value $X_{d(n)}$ exceeds 10^3 (the upper approximation limit) at about 7.8 GHz. The rest of the function values in Figs. 2c) and 2d) are within the approximation limits. The behavior of the characteristics of approximation errors can be described as follows.

The biggest values of approximation errors appear close to the approximation limits. The peak values of the approximation error for the 3rd scenario are the consequence of the approximated value being 0 (the absolute error value remains very small). After the limits of approximation variables are exceeded, the value of the approximation error grows to an undesired level. When the values of approximation variables are within and not close to the limit values, the absolute value of the approximation error is under 1%, mostly under 0.5%.

On the basis of these observations, we can provide guidance on controlling the frequency band of an UWB pulse and geometrical parameters of the creeping ray scenario in order to keep the validity of approximations.

The approximations (38) – (43) are valid when the following inequalities are fulfilled (f_L and f_H are the lower and upper limits of the considered frequency band of an input signal):

$$\frac{10^{-8}}{2\pi f_L} \le X_{wd(n)} \le \frac{10^{3}}{2\pi f_H}, \tag{45}$$

$$\frac{10^{-8}}{2\pi f_L} \le X_{wZ(n)} \le \frac{10^{3}}{2\pi f_H}, \tag{46}$$

$$\frac{10^{-11}}{2\pi f_L} \le \xi_{wd(n)} \le \frac{10^{3}}{2\pi f_H}. \tag{47}$$

Notice that variables $X_{wd(n)}$, $X_{wZ(n)}$, $\xi_{wd(n)}$ comprise only the geometry parameters of the channel. Therefore such a system of inequalities can be used to test if for a specific convex object a given ray transfer function can be approximated by (38) – (43).

IV. MODELING OF THE CHANNEL IN SPICE SIMULATOR

As a result of the approximation, described in the previous section, we obtain six transfer functions: $H_{A1(n)}(s)$, $H_{A2(n)}(s)$, $H_{Z1(n)}(s)$, $H_{Z2(n)}(s)$, $H_{D1(n)}(s)$ and $H_{D2(n)}(s)$, as a finite series of partial fractions. The single fraction, or a couple of complex conjugate fractions, represents a partial transfer function of the two-ports, which are next used to build the subcircuits corresponding to each partial transfer function. The transfer function of the three possible two-ports has one of the following forms:

$$\begin{aligned} H_{1(k)}(s) &= \frac{R_k}{s+p_k}, \\ H_{2(k)}(s) &= \frac{sR_k}{s+p_k}, \\ H_{3(k)}(s) &= \frac{R_k}{s+p_k} + \frac{R_k^*}{s+p_k^*} = \frac{b_{1k}s + b_{0k}}{s^2 + a_{1k}s + a_{0k}}. \end{aligned} \tag{48}$$

The transfer function of each two-port in (48) is a function of Laplace complex variable "s" (jω = s).

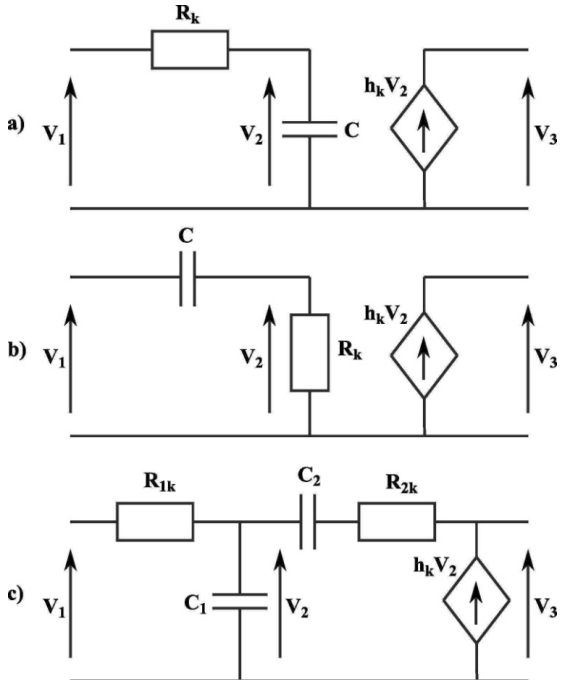

Fig.3. Two-ports corresponding to transfer functions: $H_{1(k)}(s)$-a), $H_{2(k)}(s)$-b), $H_{3(k)}(s)$-c).

The two-ports corresponding to transfer functions $H_{1(k)}(s)$, $H_{2(k)}(s)$, $H_{3(k)}(s)$ are shown in Fig. 3. a, b, c. The values of the circuit parameters are determined by the poles and the residues, which are fixed, and by the geometry of the channel scenario, which may vary from obstacle to obstacle in the cascade. Parameters R_k and p_k in (38) depend not only on residues and poles but also on geometrical parameters of a given obstacle (e.g. $R_k = CT_{1(k)} \cdot X_{wd(n)}^{-1}$ and $p_k = AT_{1(k)} \cdot X_{wd(n)}^{-1}$ in (38)). Assuming that parameters R_k and p_k are known, we can calculate the value of circuit elements in Fig. 3. a, b, c in the following way:

$$\begin{aligned} &C = C_0 = 10\text{pF}, \quad R_k = \frac{1}{C_0 p_k}, \quad h_k = \frac{R_k}{p_k} \qquad \text{a)} \\ &C = C_0 = 10\text{pF}, \quad R_k = {}^{1}\!/_{C_0 p_k}, \quad h_k = \frac{R_k}{p_k} \qquad \text{b)} \end{aligned} \tag{49}$$

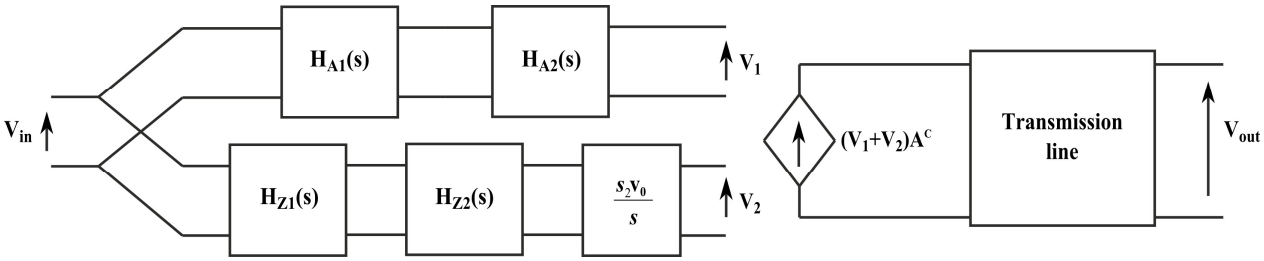

Fig. 4. Circuit equivalent to each ray for the case of two objects, two-port with transfer function s_2v_o/s denotes an integrator.

and

$$R_{2k}C_1 = 1,\ h_k = b_{1k},\ \frac{h_k}{C_2} = b_{0k},$$
$$\frac{R_{2k}}{R_{1k}} + \frac{C_2}{C_1} = a_{1k}, \frac{1}{R_{1k}C_2} + 1 - h_k = a_{0k}. \quad \text{c)} \quad (50)$$

We choose arbitrarily C_0 = 10pF. To obtain a circuit equivalent to each ray we need to connect subcircuits (equivalent to each partial transfer function) in a way resulting from general formula (2). For the case of two obstacles (N=2) the circuit equivalent to one creeping ray has the structure shown in Fig. 4. In Fig. 4 voltage V_{in} corresponds to the electric field at the output of the transmitting antenna, and the output voltage V_{out} represents the electric field at the input of the receiving antenna. The transmission line corresponds to delay expression $exp\left(-s\cdot\frac{s^p}{v_0}\right)$ in (1) and coefficient A^c is the spreading factor in the same equation. Prior to constructing a model for each creeping ray we need to check for every obstacle if parameters $X_{wd(n)}$, $X_{wZ(n)}$ and $\xi_{wd(n)}$ are in the proper range (see (45) – (47)), which guarantees that the approximation error is acceptable.

V. EXAMPLES

In this section we verify the results presented in Sections 3 and 4 through simulations of TM polarised EM wave propagating through the UWB channel containing convex obstacles. In the following examples we use values of poles and residues given in Tables I – X which are placed in APPENDIX II of the paper. We present three configurations of channels with two and three obstacles. In the UWB transmission, fast, rapidly changing signals are used. As an input signal we use an UWB pulse given by (51) with t_c=1ns and a=0.2ns:

$$p(t) = \left(1 - 4\pi\left(\frac{t-t_c}{a}\right)^2\right)\times \times exp\left(-2\pi\left(\frac{t-t_c}{a}\right)^2\right)u(t), \quad (51)$$

where u(t) is the unit step function. The shape of the pulse is shown in Fig. 5.

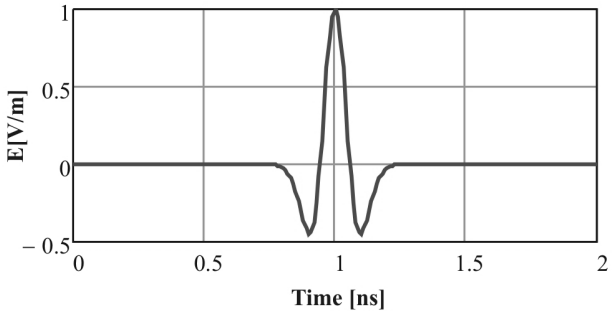

Fig. 5. The shape of the incident pulse used in simulation.

Prior to simulation or calculations of the signal propagation through the channel, we have to check that the bandwidth of the transmitted pulse and the geometry of the cascade of obstacles comply with the ranges of the variables (35) – (37) given by inequalities (45) – (47).

The lower and upper frequency band occupied by the transmitted pulse is usually known. If it is not, we set the frequencies, lower f_L and upper f_H, as these for which the amplitude of input signal in frequency domain decreases to 2% of its maximum value.

Knowing f_L we make sure that it meets the criterion of applicability of the UTD (which is usually met). Then we check the conditions of approximation given by inequalities (45) – (47) for frequency independent variables $X_{wd(n)}$, $X_{wZ(n)}$, $\xi_{wd(n)}$ (35) – (37) for all objects and rays of the given scenario. If the conditions are met we can use the tables given in APPENDIX II.

As an illustration, we give the values of geometry-dependent variables $X_{wd(n)}$, $X_{wZ(n)}$, $\xi_{wd(n)}$ for each diffraction ray case to check if they comply with inequalities (45) – (47). The values of frequencies f_L and f_H for the UWB pulse used in simulation are 0.32 GHz and 10.40 GHz, respectively. For these frequencies, $10^{-8}/2\pi f_L = 4.97\cdot10^{-18}$, $10^{-11}/2\pi f_L = 4.97\cdot10^{-21}$, $10^3/2\pi f_H = 1.53\cdot10^{-8}$. In presenting the values of $X_{wd(n)}$, $X_{wZ(n)}$, $\xi_{wd(n)}$, we use the upper index *i* and lower index *n* to indicate the ray (index *i*) and the obstacle (index *n*) to which the value corresponds.

The figures presenting the simulations results of each example include two waveforms. The solid line waveforms are calculated by IFFT of exact expressions (8), (18), (19), (22), (25), (31) while the dotted line waveforms are obtained according to the VF algorithm (Section 3) and SPICE simulation considered in Section 4.

A. Example 1

The scenario of Example 1 is shown in Fig. 6 and the corresponding results in Figs. 7 and 8. In this case, we assume that the second obstacle is rotated, α_2=-0.3rad (see Fig. 1). We consider 4 rays in the figure, denoted by nos. 1 to 4. Ray no. 1 creeps the second obstacle along almost 0 distance, therefore the approximation variables assume the values near the lower approximation limit (the approximation error takes its biggest values, see Fig. 2 and the corresponding analysis). In this example, variables $X_{wd(n)}$, $X_{wZ(n)}$, $\xi_{wd(n)}$ take the following values:
$X^1_{wd(1)} = 3.136 \cdot 10^{-10}$, $X^1_{wZ(1)} = 4.645 \cdot 10^{-10}$, $\xi^1_{wd(1)} = 6.57 \cdot 10^{-11}$, $X^1_{wd(2)} = 1.24 \cdot 10^{-16}$, $X^1_{wZ(2)} = 2.125 \cdot 10^{-16}$, $\xi^1_{wd(2)} = 1.108 \cdot 10^{-20}$, $X^2_{wd(1)} = 3.126 \cdot 10^{-10}$, $X^2_{wZ(1)} = 4.566 \cdot 10^{-10}$, $\xi^2_{wd(1)} = 6.801 \cdot 10^{-11}$, $X^2_{wd(2)} = 1.531 \cdot 10^{-10}$, $X^2_{wZ(2)} = 2.687 \cdot 10^{-10}$, $\xi^2_{wd(2)} = 1.912 \cdot 10^{-11}$, $X^3_{wd(1)} = 9.462 \cdot 10^{-10}$, $X^3_{wZ(1)} = 1.363 \cdot 10^{-9}$, $\xi^3_{wd(1)} = 4.15 \cdot 10^{-10}$, $X^3_{wd(2)} = 1.161 \cdot 10^{-9}$, $X^3_{wZ(2)} = 2.076 \cdot 10^{-9}$, $\xi^3_{wd(2)} = 4.045 \cdot 10^{-10}$, $X^4_{wd(1)} = 9.218 \cdot 10^{-10}$, $X^4_{wZ(1)} = 1.34 \cdot 10^{-9}$, $\xi^4_{wd(1)} = 3.848 \cdot 10^{-10}$, $X^4_{wd(2)} = 5.088 \cdot 10^{-10}$, $X^4_{wZ(2)} = 8.93 \cdot 10^{-10}$, $\xi^4_{wd(2)} = 1.154 \cdot 10^{-10}$.

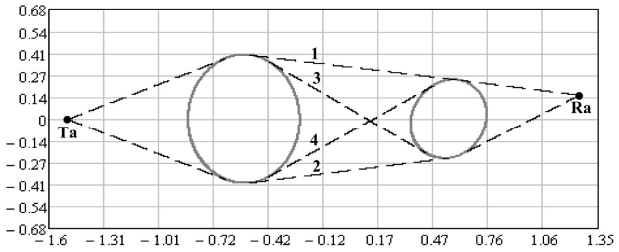

Fig. 6. Scenario of TM wave propagation on two elliptical cylinders with parameters: a_1=0.3m, b_1=0.4m, α_1=0rad , a_2=0.2m, b_2=0.25m, α_2=-0.3rad (see Fig. 1). Positions of cylinders centers are: (-0.55,0.1)m, (0.55,0)m. Positions of transmitting and receiving antenna points are (-1.5,0) and (1.25,0.1508) respectively.

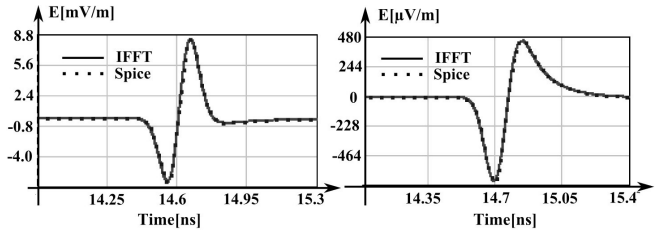

Fig. 7. Distorted components of signal received along ray no. 1 (left waveforms) and ray no. 2 (right waveforms) in scenario from Fig. 6.

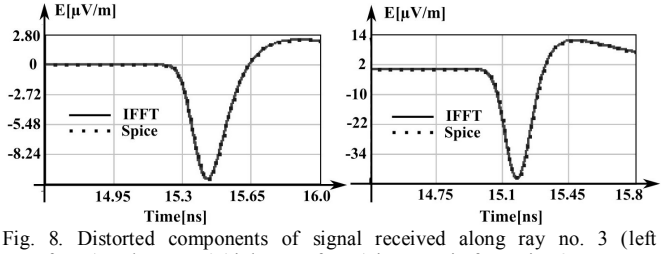

Fig. 8. Distorted components of signal received along ray no. 3 (left waveforms) and ray no. 4 (right waveforms) in scenario from Fig. 6.

B. Example 2

The scenario of Example 2 is shown in Fig. 9 and the corresponding results in Fig. 10. In this example, we have three obstacles. The transmitter and the receiver are positioned in such a way that ray no. 1 is traveling the second obstacle along a small angle distance, while the third obstacle along much greater angle distance. Ray no. 2 is creeping the first obstacle along a greater angle distance than the second one. The dominant UWB signal component is propagating along ray no. 1. In the case of ray no. 1, the calculated by us values error of approximations described in Section III is bigger than in the case of ray no. 2. (the approximation variables assume the values near the upper approximation limit). Transfer function $H_{D(n)}(\omega)$ does not appear in the transfer functions of the rays (see (6)). In this example, variables $X_{wd(n)}$, $X_{wZ(n)}$, $\xi_{wd(n)}$ take the following values:
$X^1_{wd(2)} = 4.397 \cdot 10^{-12}$, $X^1_{wZ(2)} = 5.579 \cdot 10^{-12}$, $\xi^1_{wd(2)} = 4.436 \cdot 10^{-13}$, $X^1_{wd(3)} = 2.406 \cdot 10^{-9}$, $X^1_{wZ(3)} = 3.825 \cdot 10^{-9}$, $\xi^1_{wd(3)} = 3.111 \cdot 10^{-9}$, $X^2_{wd(1)} = 3.955 \cdot 10^{-11}$, $X^2_{wZ(1)} = 5.773 \cdot 10^{-11}$, $\xi^2_{wd(1)} = 6.303 \cdot 10^{-12}$, $X^2_{wd(2)} = 6.622 \cdot 10^{-12}$, $X^2_{wZ(2)} = 1.101 \cdot 10^{-11}$, $\xi^2_{wd(2)} = 1.204 \cdot 10^{-12}$.

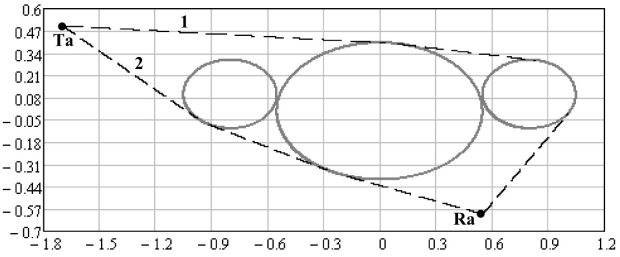

Fig. 9. Scenario of TM wave propagation on three elliptical cylinders with parameters: a_1=0.25m, b_1=0.2m, α_1=0rad, a_2=0.55, b_2=0.4m, α_2=0rad, a_3=0.25m, b_3=0.2m, α_3=0rad (see Fig. 1). Positions of cylinders centers are: (-0.8,0.1)m, (-0,0)m, (0.8,0.1)m. Positions of transmitting and receiving antenna points are (-1.7,0.5)m and (0.55,-0.6)m, respectively.

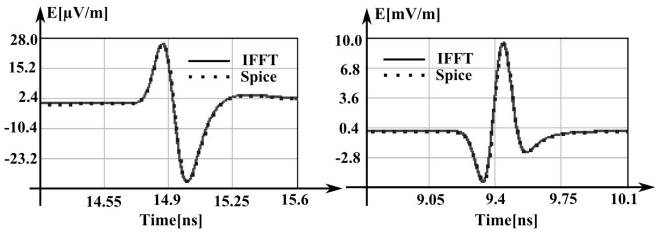

Fig. 10. Distorted components of signal received along ray no. 1 (left waveforms) and ray no. 2 (right waveforms) in scenario from Fig. 9.

C. Example 3

The scenario of Example 3 is shown in Fig. 11 and the corresponding results in Fig. 12. In this example, we have three obstacles, but in contrast to Example 2, transfer function $H_{D(n)}(\omega)$ does appear in the transfer functions of the rays. We included two dominant ray paths in the example. Transmitter and receiver are positioned in such a way that for the case of ray no. 1. the approximation variables assume smaller values than for the case of ray no. 2. For both rays the approximation variables assume the values not near approximation limits. The calculated by us values of approximation errors are below

1%. In this example, variables $X_{wd(n)}$, $X_{wZ(n)}$, $\xi_{wd(n)}$ take the following values:

$X^1_{wd(1)} = 4.98 \cdot 10^{-12}$, $X^1_{wZ(1)} = 7.151 \cdot 10^{-12}$, $\xi^1_{wd(1)} = 1.385 \cdot 10^{-13}$, $X^1_{wd(2)} = 1.967 \cdot 10^{-11}$, $X^1_{wZ(2)} = 3.533 \cdot 10^{-11}$, $\xi^1_{wd(2)} = 8.688 \cdot 10^{-13}$, $X^1_{wd(3)} = 3.239 \cdot 10^{-12}$, $X^1_{wZ(3)} = 4.624 \cdot 10^{-12}$, $\xi^1_{wd(3)} = 4.395 \cdot 10^{-14}$, $X^2_{wd(1)} = 8.047 \cdot 10^{-11}$, $X^2_{wZ(1)} = 1.149 \cdot 10^{-10}$, $\xi^2_{wd(1)} = 9.269 \cdot 10^{-12}$, $X^2_{wd(2)} = 1.123 \cdot 10^{-10}$, $X^2_{wZ(2)} = 1.995 \cdot 10^{-10}$, $\xi^2_{wd(2)} = 1.178 \cdot 10^{-11}$, $X^2_{wd(3)} = 6.032 \cdot 10^{-11}$, $X^2_{wZ(3)} = 8.685 \cdot 10^{-11}$, $\xi^2_{wd(3)} = 3.6 \cdot 10^{-12}$

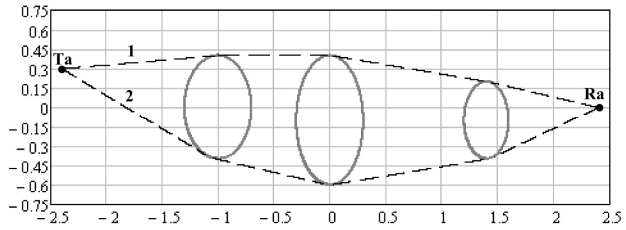

Fig. 11. Scenario of TM wave propagation on three elliptical cylinders with parameters: a_1=0.3m, b_1=0.4m, α_1=0rad , a_2=0.3, b_2=0.5m, α_2=0rad, a_3=0.2m, b_3=0.3m, α_3=0rad (see Fig. 1). Positions of cylinders centers are: (-1,0)m, (-0,-0.1)m, (1.4,-0.1)m. Positions of transmitting and receiving antenna points are (-2.4,0.3)m and (2.4,-0)m, respectively.

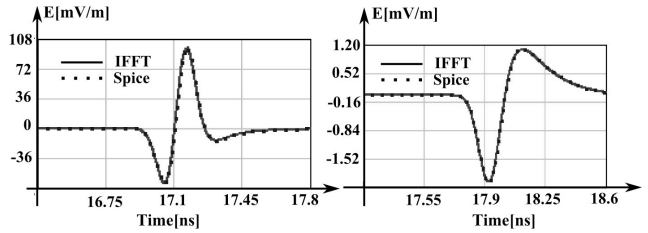

Fig. 12. Distorted components of signal received along ray no 1 (left waveforms) and ray no. 2 (right waveforms) in scenario from Fig. 11.

In the examples we compared IFFT and Spice simulation results for the rays for which the values of approximation error assume the biggest values (approximation variables assume the values near approximation limits) as well as for the rays for which the values of approximation errors are below 1%. In all examples we can see that IFFT and SPICE simulation results are in very good agreement. In all examples the ranges of $X_{wd(n)}$, $X_{wZ(n)}$, $\xi_{wd(n)}$ for given ray scenarios comply with inequalities (45) – (47) which give the limits for application of our universal approximations (38) – (43).

VI. Conclusions

In the paper we presented a universal rational approximation of the transfer function of the creeping ray for the case of UWB channels containing a cascade of convex obstacles. The approximation is performed using the vector fitting algorithm. The resulting poles and residues are independent of the geometry of objects in the cascade and of the frequency band (of course within reasonable limits). In order to obtain the universal vector fitting approximation we introduced the new variables. We specified the ranges of these new variables (VF approximation domain limits) that reflect the practical values of the UWB channel parameters. The new approximated transfer functions have the form of a finite series of partial fractions. All the poles and residues of the transfer functions for the TM polarisation case are given in the APPENDIX II of the paper. Various considered scenarios of the channel and various frequency bands can be modeled by using given poles and residues by controlling only the geometrical parameters of the scenarios (R_n, θ_n etc.).

The presented impulse response of a creeping ray has a very simple form, given by a sum of exponential functions. Therefore the obtained results are suitable for modeling an UWB channel containing a cascade of convex obstacles in SPICE-like simulators. We give examples of such modeling. The great advantage of modeling in SPICE is the possibility of including detailed models of transmitter and receiver that consider their nonlinearities. Moreover in simulations of EM wave propagation we can implement very fast and effective convolution algorithms with any input signal [20, 21]. If the incident UWB pulse is defined by the sum of exponential functions, one only needs to perform analytical calculations in order to find the shape of a signal distorted by obstacles in a channel. Our analysis and simulation results show that we offer a universal tool, basing on which everybody can model their own channel and frequency band scenarios.

Appendix I – Definitions of variables used in the paper

The definitions of variables used in the paper are as follows:

$$T_{c(n)} = \frac{1}{\sqrt{[a_n sin(\gamma_n')]^2 + [b_n cos(\gamma_n')]^2}} \times \frac{1}{\sqrt{[a_n sin(\gamma_n)]^2 + [b cos(\gamma_n)]^2}}, \tag{52}$$

$$F_{c(n)} = \left| \int_{\gamma_{n'}}^{\gamma_n} \frac{1}{\sqrt{[a_n sin(\gamma)]^2 + [b_n cos(\gamma)]^2}} \right| d\gamma, \tag{53}$$

$$G_{c(n)} = a_n b_n F_{c(n)} \sqrt{\frac{T_{c(n)}}{2V_0}}, \tag{54}$$

$$K_{11(n)} = \frac{1}{\sqrt{[a_n sin(\gamma_n)]^2 + [b_n cos(\gamma_n)]^2} F_{c(n)}} - \frac{1}{4} \frac{|sin(2\gamma_n)|(a_n{}^2 - b_n{}^2)}{[a_n sin(\gamma_n)]^2 + [b_n cos(\gamma_n)]^2}, \tag{55}$$

$$K_{12(n)} = \frac{-1}{\{[a_n sin(\gamma_n)]^2 + [b_n cos(\gamma_n)]^2\} F_{c(n)}{}^2} - \frac{1}{2} \frac{|sin(2\gamma_n)|(a_n{}^2 - b_n{}^2)}{\{[a_n sin(\gamma_n)]^2 + [b_n cos(\gamma_n)]^2\}^{\frac{3}{2}} F_{c(n)}} - \frac{(a_n{}^2 - b_n{}^2)}{2} \frac{|cos(2\gamma_n)|}{[a_n sin(\gamma_n)]^2 + [b_n cos(\gamma_n)]^2} + \frac{(a_n{}^2 - b_n{}^2)}{4} \frac{sin(2\gamma_n)^2 (a_n{}^2 - b_n{}^2)}{\{[a_n sin(\gamma_n)]^2 + [b_n cos(\gamma_n)]^2\}^2}, \tag{56}$$

$$K_{2(n)} = \frac{2|cos(2\gamma_n)|}{\{[a_n sin(\gamma_n)]^2 + [b_n cos(\gamma_n)]^2\}^{\frac{3}{4}}} - \frac{3}{4} \frac{sin(2\gamma_n)^2 (a_n{}^2 - b_n{}^2)}{\{[a_n sin(\gamma_n)]^2 + [b_n cos(\gamma_n)]^2\}^{\frac{7}{4}}}. \tag{57}$$

APPENDIX II– POLES AND RESIDUES OF UNIVERSAL APPROXIMATIONS

All the poles and residues that we used in (38) – (43) are given in Tables I – X. The names of poles and residues used in the tables are the same as in (38) – (43). The numbers of poles and residues are the result of a compromise between the accuracy of approximation and complexity of the formulas. Most of the poles and residues in tables are real but some of them take the form of complex conjugate pairs. Therefore, it is enough to give one pair: residue, pole, e.g. $R_k = R_k^{re} + jR_k^{im}$, $p_k = p_k^{re} + jp_k^{im}$ because the second pair $R_{k+1} = R_k^{re} - jR_k^{im}$, $p_{k+1} = p_k^{re} - jp_k^{im}$ is a complex conjugate. Exactly as for example in Table 1, where there are given pairs: (R_{33}, p_{33}), (R_{35}, p_{35}), (R_{37}, p_{37}), (R_{39}, p_{39}), which are respectively equal to $R_{34} = R_{33}^*$, $p_{34} = p_{33}^*$ etc. (* denotes a complex conjugate).

TABLE I
VALUES OF POLES DENOTED BY AF1 USED IN (39), (40) AND (43)

$AF1_1$	-6.223085189161760E-12	$AF1_2$	-4.642943424752610E-11
$AF1_3$	-2.632971537519530E-10	$AF1_4$	-1.455675152126270E-09
$AF1_5$	-7.835948594742870E-09	$AF1_6$	-4.038813536555160E-08
$AF1_7$	-1.968546136481600E-07	$AF1_8$	-9.017520026176850E-07
$AF1_9$	-3.880429205437380E-06	$AF1_{10}$	-1.575218154451000E-05
$AF1_{11}$	-6.080931050595430E-05	$AF1_{12}$	-2.258657597275270E-04
AF_{13}	-8.185450184600070E-04	$AF1_{14}$	-2.909960541822810E-03
$AF1_{15}$	-4.387393681132390E-03	$AF1_{16}$	-9.888524748122700E-03
$AF1_{17}$	-3.076293295546190E-02	$AF1_{18}$	-5.319820485776900E-02
$AF1_{19}$	-8.530038238164280E-02	$AF1_{20}$	-2.107537360374780E-01
$AF1_{21}$	-4.852919518921980E-01	$AF1_{22}$	-1.109240947443870E+00
$AF1_{23}$	-2.555612087490020E+00	$AF1_{24}$	-5.971938758773050E+00
$AF1_{25}$	-1.376184845890750E+01	$AF1_{26}$	-3.152721189756180E+01
$AF1_{27}$	-7.135894598273800E+01	$AF1_{28}$	-1.525677339536200E+02
$AF1_{29}$	-3.263092485757550E+02	$AF1_{30}$	-7.215703463100180E+02
$AF1_{31}$	-1.959987932375670E+03	$AF1_{32}$	-1.609740959845480E+04
$Re(AF1_{33})$	-4.561149007155700E-01	$Im(AF1_{33})$	3.759847198447340E+00
$Re(AF1_{35})$	-2.234456627061440E-02	$Im(AF1_{35})$	6.279323246956080E+00
$Re(AF1_{37})$	-4.329006283843410E-01	$Im(AF1_{37})$	6.918866479018330E+00
$Re(AF1_{39})$	-7.023421504553170E-02	$Im(AF1_{39})$	7.845889264970790E+00

TABLE II
VALUES OF RESIDUES DENOTED BY CF1 USED IN (39), (40) AND (43)

$CF1_1$	-7.117913128279230E-11	$CF1_2$	-2.418081305008450E-10
$CF1_3$	-1.009872969604920E-09	$CF1_4$	-4.136056787649920E-09
$CF1_5$	-1.650884157500870E-08	$CF1_6$	-6.275930275111510E-08
$CF1_7$	-2.265204113568500E-07	$CF1_8$	-7.735262801933800E-07
$CF1_9$	-2.509836311660360E-06	$CF1_{10}$	-7.785785657013580E-06
$CF1_{11}$	-2.335976441528150E-05	$CF1_{12}$	-6.863118137244520E-05
$CF1_{13}$	-2.008412931521980E-04	$CF1_{14}$	-5.741662909540510E-04
$CF1_{15}$	-5.531723198923410E-06	$CF1_{16}$	-1.551618675371540E-03
$CF1_{17}$	-3.817058019141940E-03	$CF1_{18}$	5.057827163347960E-05
$CF1_{19}$	-8.303193175562140E-03	$CF1_{20}$	-1.642642304640750E-02
$CF1_{21}$	-3.320881340611830E-02	$CF1_{22}$	-6.899626028833290E-02
$CF1_{23}$	-1.392889335153080E-01	$CF1_{24}$	-2.497718979548050E-01
$CF1_{25}$	-3.355045406579710E-01	$CF1_{26}$	-3.856566272181840E-01

TABLE II – CONT.

$CF1_{27}$	-5.716422546437500E-01	$CF1_{28}$	-8.537999105459460E-01
$CF1_{29}$	-1.236874679092110E+00	$CF1_{30}$	-2.042323446540440E+00
$CF1_{31}$	-4.981162295862690E+00	$CF1_{32}$	-4.477523011713860E+01
$Re(CF1_{33})$	1.667279203879630E-06	$Im(CF1_{33})$	4.335171598911150E-09
$Re(CF1_{35})$	1.604020576259050E-09	$Im(CF1_{35})$	-1.680504157973360E-07
$Re(CF1_{37})$	1.910068214302970E-06	$Im(CF1_{37})$	-6.893633467605250E-06
$Re(CF1_{39})$	8.509276835837030E-08	$Im(CF1_{39})$	1.962641959724880E-09

TABLE III
VALUES OF POLES DENOTED BY AF2 USED IN (40)

$AF2_1$	-1.3746615524148000E+04	$AF2_2$	-1.674374835871920E+03
$AF2_3$	-6.043228594262280E+02	$AF2_4$	-2.610728121202200E+02
$AF2_5$	-1.268656144255840E+02	$AF2_6$	-5.003724628994100E+01
$AF2_7$	-2.442485304632910E+01	$AF2_8$	-1.284086824715810E+01
$AF2_9$	-6.606262256604180E+00	$AF2_{10}$	-3.279206438784520E+00
$AF2_{11}$	-7.326939942939360E-01	$AF2_{12}$	-3.401865368490160E-01
$AF2_{13}$	-1.569748272087090E-01	$AF2_{14}$	-7.177472500823550E-02
$AF2_{15}$	-3.242867313993420E-02	$AF2_{16}$	-1.443392990795180E-02
$AF2_{17}$	-6.309918390574090E-03	$AF2_{18}$	-2.701779047307750E-03
$AF2_{19}$	-1.130347827990600E-03	$AF2_{20}$	-4.610867318301980E-04
$AF2_{21}$	-1.830264944560560E-04	AF_{22}	-7.056616704972060E-05
AF_{23}	-2.637692940064010E-05	$AF2_{24}$	-9.540518946925170E-06
$AF2_{25}$	-3.332624885957460E-06	$AF2_{26}$	-1.121993575638200E-06
$AF2_{27}$	-3.633301526188140E-07	$AF2_{28}$	-1.129444009107950E-07
$AF2_{29}$	-3.364328423774080E-08	$AF2_{30}$	-9.588483206081420E-09
$AF2_{31}$	-2.611890071597190E-09	$AF2_{32}$	-6.796188658473310E-10
$AF2_{33}$	-1.687836501224450E-10	$AF2_{34}$	-3.951019164709950E-11
$AF2_{35}$	-7.016868795174380E-12	$AF2_{36}$	---

TABLE IV
VALUES OF RESIDUES DENOTED BY CF2 USED IN (40)

$CF2_1$	4.132325813048490E+01	$CF2_2$	4.637660008655480E+00
$CF2_3$	1.932943430943590E+00	$CF2_4$	1.180504957639740E+00
$CF2_5$	7.520467883771120E-01	$CF2_6$	3.089399120014710E-01
$CF2_7$	6.033682590790940E-01	$CF2_8$	4.700371971782570E-01
$CF2_9$	1.962449181302360E-01	$CF2_{10}$	4.564635729802700E-02
$CF2_{11}$	-5.896274423153400E-03	$CF2_{12}$	-3.852270965656500E-03
$CF2_{13}$	-1.897349930022360E-03	$CF2_{14}$	-8.388339558475660E-04
$CF2_{15}$	-3.507356058098300E-04	$CF2_{16}$	-1.414643083041700E-04
$CF2_{17}$	-5.543667713625890E-05	$CF2_{18}$	-2.114611732489110E-05
$CF2_{19}$	-7.848021903383540E-06	$CF2_{20}$	-2.829964691846890E-06
$CF2_{21}$	-9.897144554887930E-07	$CF2_{22}$	-3.350235956701320E-07
$CF2_{23}$	-1.095331233355760E-07	$CF2_{24}$	-3.450907616752520E-08
$CF2_{25}$	-1.045193288090630E-08	$CF2_{26}$	-3.035624588164280E-09
$CF2_{27}$	-8.432738255859820E-10	$CF2_{28}$	-2.234871040649260E-10
$CF2_{29}$	-5.636862515468340E-11	$CF2_{30}$	-1.350233188300650E-11
$CF2_{31}$	-3.066210007384750E-12	$CF2_{32}$	-6.595507506982490E-13
$CF2_{33}$	-1.343812414057510E-13	$CF2_{34}$	-2.619271660646870E-14
$CF2_{35}$	-5.238444753597610E-15	$CF2_{36}$	---

TABLE V

VALUES OF POLES DENOTED BY AF3 USED IN (43)

$AF3_1$	-1.860704688368650E+04	$AF3_2$	-2.236833326596330E+03
$AF3_3$	-8.354589773292290E+02	$AF3_4$	-3.870090454083990E+02
$AF3_5$	-2.148960953335420E+02	$AF3_6$	-9.088827518542690E+01
$AF3_7$	-4.545801963472270E+01	$AF3_8$	-2.949387754632620E+01
$AF3_9$	-1.840507415386010E+01	$AF3_{10}$	-6.545000109157150E+00
$AF3_{11}$	-3.745131929694850E+00	$AF3_{12}$	-2.092371723823880E+00
$AF3_{13}$	-1.144443031250800E+00	$AF3_{14}$	-6.141107284157960E-01
$AF3_{15}$	-3.238790384321420E-01	$AF3_{16}$	-1.682027450827290E-01
$AF3_{17}$	-8.614847753783800E-02	$AF3_{18}$	-4.343945536386370E-02
$AF3_{19}$	-2.135461399794560E-02	$AF3_{20}$	-1.003896673503620E-02
$AF3_{21}$	-1.824363124211580E-03	$AF3_{22}$	-7.162560334679940E-04
$AF3_{23}$	-2.729350845495800E-04	$AF3_{24}$	-1.016593727211750E-04
$AF3_{25}$	-3.698754549558320E-05	$AF3_{26}$	-1.310384679111750E-05
$AF3_{27}$	-4.502930012156680E-06	$AF3_{28}$	-1.494421086094840E-06
$AF3_{29}$	-4.765892658354140E-07	$AF3_{30}$	-1.451387018478390E-07
$AF3_{31}$	-4.186166203827170E-08	$AF3_{32}$	-1.130755797239390E-08
$AF3_{33}$	-2.815346525612970E-09	$AF3_{34}$	-6.311535207669710E-10
$AF3_{35}$	-1.224659001541020E-10	$AF3_{36}$	-1.852426043844880E-11

TABLE VI

VALUES OF RESIDUES DENOTED BY CF3 USED IN (43)

$CF3_1$	-9.662659402489120E+01	$CF3_2$	-1.066087624334810E+01
$CF3_3$	-4.283964665282770E+00	$CF3_4$	-2.248179819422330E+00
$CF3_5$	-2.540388984118260E+00	$CF3_6$	9.932854062205620E-01
$CF3_7$	-1.802003281904000E+00	$CF3_8$	-2.363418248137430E+00
$CF3_9$	-1.086362142349220E+00	$CF3_{10}$	2.759345158207460E-01
$CF3_{11}$	1.935925403061090E-01	$CF3_{12}$	8.831781929101930E-02
$CF3_{13}$	3.256300280393410E-02	$CF3_{14}$	1.054399452373690E-02
$CF3_{15}$	3.119690380932170E-03	$CF3_{16}$	8.594297800153410E-04
$CF3_{17}$	2.217664806662160E-04	$CF3_{18}$	5.308738855902490E-05
$CF3_{19}$	1.120062702979670E-05	$CF3_{20}$	1.713291137758090E-06
$CF3_{21}$	-1.195615466019360E-07	$CF3_{22}$	-5.342299475835860E-08
$CF3_{23}$	-1.687765247147720E-08	$CF3_{24}$	-4.591110169957410E-09
$CF3_{25}$	-1.140317413361050E-09	$CF3_{26}$	-2.639087713359640E-10
$CF3_{27}$	-5.729975732321290E-11	$CF3_{28}$	-1.168209429901330E-11
$CF3_{29}$	-2.230583133384090E-12	$CF3_{30}$	-3.966456363081020E-13
$CF3_{31}$	-6.508786867434540E-14	$CF3_{32}$	-9.725031464443260E-15
$CF3_{33}$	-1.295843539617210E-15	$CF3_{34}$	-1.496738502618100E-16
$CF3_{35}$	-1.418855685351500E-17	$CF3_{36}$	-1.056245229910440E-18

TABLE VII

VALUES OF POLES DENOTED BY AT1 USED IN (38), (40) AND (42)

$AT1_1$	-3.468072678938460E+04	$AT1_2$	-4.084329133987000E+03
$AT1_3$	-1.563781940600060E+03	$AT1_4$	-8.097411700739480E+02
$AT1_5$	-4.648224593792050E+02	$AT1_6$	-2.759147884142890E+02
$AT1_7$	-1.648093132313600E+02	$AT1_8$	-9.793125301195320E+01
$AT1_9$	-5.757464436583650E+01	$AT1_{10}$	-3.338519930673860E+01
$AT1_{11}$	-1.905323688992640E+01	$AT1_{12}$	-1.068970034420490E+01
$AT1_{13}$	-5.903041999379620E+00	$AT1_{14}$	-3.236447835934380E+00
$AT1_{15}$	-1.771228217479420E+00	$AT1_{16}$	-9.571358439533220E-01
$AT1_{17}$	-5.038358907359960E-01	$AT1_{18}$	-2.556963196795430E-01
$AT1_{19}$	-1.240265540512290E-01	$AT1_{20}$	-5.698552251049420E-02

TABLE VII – CONT.

$AT1_{21}$	-2.453312246336900E-02	$AT1_{22}$	-9.755291375604240E-03
$AT1_{23}$	-3.511928195804320E-03	$AT1_{24}$	-1.111810574755850E-03
$AT1_{25}$	-2.959745873565210E-04	$AT1_{26}$	-6.149879155844460E-05
$AT1_{27}$	-8.666973552989780E-06	$AT1_{28}$	-5.928456049462410E-07

TABLE VIII

VALUES OF RESIDUES DENOTED BY CT1 USED IN (38), (40) AND (42)

$CT1_1$	2.350146540529970E+02	$CT1_2$	2.569344209997450E+01
$CT1_3$	9.518831670509370E+00	$CT1_4$	5.338428179924050E+00
$CT1_5$	3.652148004144690E+00	$CT1_6$	2.731594346342210E+00
$CT1_7$	2.117862278643390E+00	$CT1_8$	1.662991063684240E+00
$CT1_9$	1.310175845384090E+00	$CT1_{10}$	1.032363118014490E+00
$CT1_{11}$	8.136967576006300E-01	$CT1_{12}$	6.444822217608520E-01
$CT1_{13}$	5.216859836779230E-01	$CT1_{14}$	4.298176301264680E-01
$CT1_{15}$	3.251647623711980E-01	$CT1_{16}$	2.059919331198440E-01
$CT1_{17}$	1.083976847120910E-01	$CT1_{18}$	4.869482665415000E-02
$CT1_{19}$	1.918760674134540E-02	$CT1_{20}$	6.739120060706360E-03
$CT1_{21}$	2.117205644374970E-03	$CT1_{22}$	5.899097160435170E-04
$CT1_{23}$	1.427686795509540E-04	$CT1_{24}$	2.894938775797240E-05
$CT1_{25}$	4.639272389233180E-06	$CT1_{26}$	5.321749855904010E-07
$CT1_{27}$	3.637819135849780E-08	$CT1_{28}$	9.541742623624040E-10

TABLE IX

VALUES OF POLES DENOTED BY AT2 USED IN (40) AND (42)

$AT2_1$	-2.737855326072540E+13	$AT2_2$	-3.245167924007200E+12
$AT2_3$	-1.235402492705890E+12	$AT2_4$	-6.236518932003150E+11
$AT2_5$	-3.444878790701270E+11	$AT2_6$	-1.960708743831270E+11
$AT2_7$	-1.127107756238660E+11	$AT2_8$	-6.499615367781200E+10
$AT2_9$	-3.751357314758990E+10	$AT2_{10}$	-2.165439301658100E+10
$AT2_{11}$	-1.249881524894190E+10	$AT2_{12}$	-7.213467742699420E+09
$AT2_{13}$	-4.162798142098850E+09	$AT2_{14}$	-2.402230341611000E+09
$AT2_{15}$	-1.386295795562500E+09	$AT2_{16}$	-8.000758315306380E+08
$AT2_{17}$	-4.618000604404720E+08	$AT2_{18}$	-2.665701815454330E+08
$AT2_{19}$	-1.538552581835530E+08	$AT2_{20}$	-8.872266161473120E+07
$AT2_{21}$	-5.100196568766890E+07	$AT2_{22}$	-2.902859757405890E+07
$AT2_{23}$	-1.603458616170280E+07	$AT2_{24}$	-8.094527966195940E+06
$AT2_{25}$	-3.081504648140490E+06	$AT2_{26}$	-3.652493964934570E+05

TABLE X

VALUES OF RESIDUES DENOTED BY CT2 USED IN (40) AND (42)

$CT2_1$	6.593459699639570E+06	$CT2_2$	7.222925926282760E+05
$CT2_3$	2.730814493211610E+05	$CT2_4$	1.565071296024100E+05
$CT2_5$	1.071062643438640E+05	$CT2_6$	7.848475502000550E+04
$CT2_7$	5.893262725074520E+04	$CT2_8$	4.462179297635840E+04
$CT2_9$	3.387746041382510E+04	$CT2_{10}$	2.573991691698900E+04
$CT2_{11}$	1.955943053076880E+04	$CT2_{12}$	1.486182750736080E+04
$CT2_{13}$	1.129108971054340E+04	$CT2_{14}$	8.577298138520720E+03
$CT2_{15}$	6.515205556793640E+03	$CT2_{16}$	4.948657051699420E+03
$CT2_{17}$	3.758903063585250E+03	$CT2_{18}$	2.855764654584920E+03
$CT2_{19}$	2.170997683966910E+03	$CT2_{20}$	1.653447326516230E+03
$CT2_{21}$	1.265820781607740E+03	$CT2_{22}$	9.831978641749930E+02
$CT2_{23}$	7.935821325764090E+02	$CT2_{24}$	6.990105422260550E+02
$CT2_{25}$	7.038433095295670E+02	$CT2_{26}$	7.615577845219540E+02

REFERENCES

[1] M.Z. Win D. Porcino, W. Hirt , "Ultra-wideband radio technology: potential and challenges ahead", *IEEE Communications Magazine*, July 2003, pp. 2-11,

[2] P. R. Rousseau, P. H. Pathak, Hsi-Tseng Chou, "A time domain formulation of the uniform geometrical theory of diffraction for scattering from a smooth convex surface", *IEEE Transactions on Antennas and Propagation*, vol. 55, no. 6, June 2007, pp. 1522-1534

[3] P. R. Rousseau, P. H. Pathak, "TD-UTD for scattering from a smooth convex surface", in *Proc. Antennas and Propagation Society International Symposium*, Baltimore, 21-26 July 1996, vol. 3, pp. 2084-2087

[4] Hsi-Tseng Chou, P.H Pathak, P. R. Rousseau, "TD-UTD Solutions for the Transient Radiation and Surface Fields of Pulsed Antennas Placed on PEC Smooth Convex Surfaces", *IEEE Transactions on Antennas and Propagation*, vol. 59, no. 5, May 2011, pp. 1626-1637

[5] Chenming Zhou, R. C. Qiu, "Pulse distortion caused by cylinder diffraction and its impact on UWB communications", in *Proc. The IEEE 2006 International Conference on Ultra-Wideband*, Waltham, MA, September 2006, pp.645-650.

[6] G. Koutitas, C. Tzaras, "A UTD Solution for Multiple Rounded Surfaces", *IEEE Transactions on Antennas and Propagation*, vol. 54, no. 4, April 2006, pp 1277-1283

[7] P. Górniak, W. Bandurski, "Direct Time Domain Analysis of an UWB Pulse Distortion by Convex Objects with the Slope Diffraction Included", *IEEE Transactions on Antennas and Propagation*, vol. 56, no. 9, September 2008, pp. 3036–3044

[8] P. Górniak, W. Bandurski, „Time Domain Transition Zone Diffraction on Convex Obstacles", in *Ultra-Wideband, Short-Pulse Electromagnetics 9*, Springer Verlag, April 2010.

[9] B. Chaudhury, P.K. Chattopadhyay, D. Raju, S. Chaturvedi, "Transient Analysis of Creeping Wave Modes Using 3-D FDTD Simulation and SVD Method", *IEEE Transactions on Antennas and Propagation*, vol. 57, no. 3, March 2009, pp. 754-759

[10] D.E. Foreman, D.F. Sedivec, "Experimental observation of the creeping-wave phenomenon in backscatter using a short-pulse radar system", in *Proceedings of the IEEE*, vol. 53, no. 8, August 1965, pp. 1102-1104

[11] K. Naishadham, J.E. Piou, "A Robust State Space Model for the Characterization of Extended Returns in Radar Target Signatures", *IEEE Transactions on Antennas and Propagation*, vol. 56, no. 6, June 2008, pp. 1742-1751

[12] A.Y. Grinev, D.V. Bagno, A.E. Zaikin, D.V. Nikishov, "Multi-channel Ground Penetrating Radar based on ultra-wideband short-pulse signal: Hardware and software", in *Proc. 13th International Conference on Ground Penetrating Radar*, Itally, Lecce, 21-25 June, 2010, pp. 1-6

[13] B. Gustavsen, A. Semlyen, "Rational approximation of frequency domain response by vector fitting", *IEEE Transactions on Power Delivery*, vol.14, no. 3, 1999, pp. 1052-1061.

[14] P. H. Pathak, W. Burnside, R. Marhefka, "A uniform GTD analysis of the diffraction of electromagnetic waves by a smooth convex surface", *IEEE Transactions on Antennas and Propagation*, vol. 28, no. 5, September 1980, pp. 631-642.

[15] D. A. McNamara, *Introduction to the uniform geometrical theory of diffraction*, Artech House, Boston, London, 1990.

[16] P. R. Rousseau, P. H. Pathak, "TD-UTD slope diffraction for a perfectly conducting curved wedge", in *Proc. Antennas and Propagation Society International Symposium*, Newport Beach, 18-23 June 1995, vol. 2, pp. 856-859

[17] M. Ghaddar, L. Talbi, T. A. Denidni, A. Sebak, "A Conducting Cylinder for Modeling Human Body Presence in Indoor Propagation channel", *IEEE Transactions on Antennas and Propagation*, vol. 55, no. 11, November 2007, pp. 3099-3103

[18] I. Kashiwagi, T. Imai, "Time-varying Path-Shadowing Model for Indoor Populated Environments", *IEEE Transactions on Vehicular Technology*, vol. 59, no. 1, January, 2010, pp. 16–29.

[19] http://www.sintef.no/Projectweb/VECTFIT/

[20] A. Semlyen, A. Dabuleanu, "Fast and Accurate Switching Transient calculation on Transmission Lines with Ground Return Using Recursive Convolution", *IEEE Transactions on Power Apparatus and Systems*, vol. PAS-94, no. 2, March 1975, pp. 561-571

[21] W. Janke, G. Blakiewicz, "Semi Analytical Recursive Algorithms for Convolution Calculations", in *Proc. IEE - Circuits, Devices and Systems*, vol. 142, no. 2, April 1995, pp. 125-130

Piotr Górniak was born in 1980. He received his M.Sc. and Ph.D. degrees from Poznan University of Technology in 2004 and 2010 respectively. Currently, he works as an assistant professor at Poznan University of Technology.

He is an author and co-author of papers and conference contributions on channel modeling as well as time-domain and frequency-domain techniques in empirical and deterministic analysis of ultra-wideband electromagnetic wave propagation. He is interested in technologies of ultra fast systems of wireless data transmission as well as high resolution radar and sensor techniques

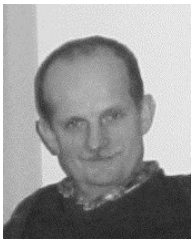

Wojciech Bandurski was born in 1946. He received M.S., Sc.D. and Habilitation degrees from Poznan University of Technology, Poland in 1970, 1979 and 1996 respectively. He was with Laboratorie d'Electromagnetisme et Acoustique, Ecole Politechnique Federale de Lausanne, Switzerland in (10.02-10.08).1992. Currently, he is a professor at Poznan University of Technology.

He is an author as well as co-author of about 100 papers and conferences contributions mostly on analytical and numerical methods in distributed circuits and systems, computer simulation of transients on interconnects in high-speed digital circuits and microwave circuits, transmission line analysis and synthesis, modeling of propagation of electromagnetic wave in UWB channels. Member of the Revision Committee of Polish Society Theoretical and Applied Electrical Engineering (PTETiS).